The influence of plasma dynamics on the growth of $Sm_{0.55}Nd_{0.45}NiO_3$ solid solution during pulsed laser deposition

B. D. Ngom[1,2,3], S. Lafane[4], A. Dioum[3], N. Manyala[5], S. Abdelli-Messaci[4], R. T. Kerdja[4], R. Madjoe[1], R. Nemutudi, M. Maaza[2], A. C. Beye[3]

[1]Department of Physics, University of the Western Cape, Cape Town, South Africa,
[2]Nanosciences Laboratories, Materials Research Group, iThemba LABS, National Research Foundation, South Africa,
[3]Groupes de physique du Solide et Sciences des Matériaux (GPSSM), Faculté des sciences et Techniques Université Cheikh Anta Diop de Dakar (UCAD) B.P. 25114 Dakar-Fann Dakar (Senegal).
[4]Centre de développement des technologies avancées, Cité 20 août 1956, B.P. 17, Baba Hassen, Algeria,
[5]Department of Physics, SARCHI Chair in Carbon Technology and Materials, Institute of Applied Materials, University of Pretoria, Pretoria, South Africa,

Abstract.

We report on the presence of an interesting cross–correlation among the deposition parameters which are usually overlooked in the usual empirical approach used by pulsed laser deposition growers. The fast intensified-charge-coupled-device (ICCD) photography imaging studies of the plasma generated by the KrF excimer laser ablation of $Sm_{1-x}Nd_xNiO_3$ at x= 0.45 in the presence of oxygen background gases at different pressures is reported. The experimentally determined behaviours are compared with the predictions of an analytical model which gives a complete description of the expansion of the plume and with some recent results reported in the literature. Evidence of the strong influence of the expansion plasma regime was found which showed that it is not simply related to the overall reactive gas content. Our findings demonstrate that the optimization of the pulsed laser deposition parameters, such as gas pressure, should be performed also taking into account the chemical pressure induced by the substrate nature. The analysis of the experimental results allowed us to estimate the average deposition oxygen pressure for $Sm_{0.55}Nd_{0.45}NiO_3$ in the typical range used for Pulsed Laser Deposition (PLD) of complex oxides, showing that the higher is the deposition pressure, the better the crystallinity.

Corresponding Author: Dr. Balla Diop Ngom, bdngom@tlabs.ac.za

Nanosciences Laboratories, Materials Research Department, iThemba LABS, National Research Foundation, P O Box 722, Somerset West, Cape Town, Western Cape 7129, South Africa. Tel.: +27218431145/46.

Introduction

Due to its Metal-Insulator Transition (MIT) and thermochromic properties, the rare earth nickelate perovskite $ReNiO_3$ (Re = rare earth) family has received a great deal of attention over the past ten years [1]. Such unusual electronic and optical features are of great interest since the Metal-Insulator Transition Temperature (T_{MIT}) can be tuned by changing the Re cation or by forming a solid solution [2-4].

The difficulty of preparing these complex rare earth nickel oxides in the series of $ReNiO_3$ increases severely as the radius of the rare earth decreases. Generally, it requires oxide reaction above 1000 $^{\circ}$C under excessive oxygen pressure of about 200 bars during several days [5-7]. Several studies have been reported also on the dynamics of the plasma plume generated by PLD of complex oxides in a background gas [8-13]. These studies showed that the dynamics of plasma plume is greatly affected by the ambient gas pressure. Only a careful control of thin film growth can therefore allow their application in the fabrication of photonic or electronic devices.

Several models have been proposed to describe the ablation plume expansion dynamic. Among the several models dealing with plume expansion, a first distinction should be done between plume expansion in vacuum and in an environmental gas. The plume expansion dynamic in vacuum was extensively investigated by Anisimov et al. [14] and by Singh and Narayan [15], resorting to a self-similar expansion of an elliptical, neutral gas cloud. The two previous cited models differ essentially for the analysis of the plume expansion during the first stage, which timescale is of the order of the laser pulse duration. Then, after the laser pulse, both models hypothesize an adiabatically expanding plume, in which the plume energy, initially purely thermal, is progressively transformed into kinetic energy during the expansion. After a short transient stage, the plume front dynamics becomes linear with respect to time, reaching a maximum, asymptotic expansion velocity. This free-plume expansion stage is reached when all the initial thermal energy has been transferred to kinetic energy of the ablated species, which travel at the asymptotic velocity during the further expansion.

Among the plume expansion models in gas [16-18], here we will shortly recall those developed by Predtechensky [17] and Arnold [16]. In both these models, the ablated materials act to sweep up the environmental gas, driving it at supersonic velocity. As consequence, a contact front is formed between the plume and the ambient gas. While the former only deals with the dynamics of the contact front, the latter also considers the internal dynamics of the plume and of the external background gas layer formed during plume-ambient gas interaction. This model refers to two regions in contact: one

on the edge of the traveling plume and the other in the ambient gas along the plume periphery. During the plume expansion, the ablated particles and the ambient gas molecules are confined and compressed in two thin layers, due to the reciprocal interaction.

The plasma expansion in a gas environment has been also described in the literature in terms of different phenomenological models depending on the experimental regimes, affected by the pressure range of the gas present during the deposition process, by the energy of the plasma species and by the temporal stage of propagation [19-25]. At low pressure and in the early times of the expansion, the plasma dynamics is in good agreement with the drag-force model [22]. In this model the ejected species are regarded as an ensemble that experiences a viscous force proportional to its velocity V through the background gas:

$$V = V_o e^{-\beta t} \qquad (1)$$

or analogously

$$R = R_o \left(1 - e^{-\beta t}\right) \qquad (2)$$

where R indicates the position of the front edge of the plasma, R_0 the distance at which the plasma propagation ceases (it is generally indicated as the stopping distance) and β a slowing coefficient. Both R_0 and β are phenomenological parameters whose values are, necessarily, determined by fitting the experimental data to Eq. (2). As reported in some works [22, 23], the estimated R_0 values are more than one order of magnitude larger than the calculated inelastic mean free path λ values. Such large differences are presumably due to the fact that R_0 is a rather complex function of several experimental parameters such as the background gas nature and pressure, the mass and the energy of the plasma and last, but not least, the (target material)/(gas specie) atomic mass ratio. The drag model holds only for low gas pressures; upon increasing the gas pressure values, this model predicts distances slightly shorter than those observed experimentally. Thus, the presence of a higher background gas pressure produces a non linear dependence on the distance from the target of the plasma front edge position. For high background pressures the plasma expansion follows the path described by the blast wave model [24, 25]. According to this model, created to describe the propagation of a shock wave through a background gas after an explosion, just after the arrival of the laser pulse on the target surface, a plasma ball develops and starts to expand along the normal to the target surface. The expanding plasma can act as a piston, compressing

and accelerating the gas molecules to a supersonic velocity, with the formation of a shock wave ahead of the contact surface between the plasma and the ambient gas.

The position of the front edge, as a function of the time t, is given by the following relation:

$$R = \xi_o \left(\frac{E}{\rho_o} \right)^{1/5} t^{2/5} \tag{3}$$

where ξ_0 (~1) is a factor related to both geometrical and thermodynamic quantities, E is the plasma energy and ρ_0 the density of the undisturbed gas. This model can strictly be applied only when the mass of the gas surrounding the shock wave is higher than the mass of the ablated material and only up to distances from the target at which the pressure driving the moving front of the plasma is greater than the pressure of the gas at rest. Then the shock wave can be observed only in a limited spatial region R:

$$\left(\frac{3M_o}{4\pi\rho_o} \right)^{1/3} << R << \left(\frac{E}{P_o} \right)^{1/3} \tag{4}$$

Where M_0 is the mass of the expanding plasma and P_0 is the pressure ahead of the shock wavefront [21, 22].

Experimentally the plasma generated in PLD experiments shows a behavior described by a mix of these two models: it starts following the drag model and then, when the viscous slowing of the plasma front edge coalesces to form the shock front, it will expand according to the blast wave model. In the last years, Arnold et al. [16] proposed an analytical approach to explain the complete dynamics of the laser generated plasma into ambient gas valid for any pressure value and for any spatial and temporal regime. This phenomenological model provides some differential equations for the characteristic radii describing the spherical plasma expansion and takes into account three different process stages: an early stage where the plasma expansion is characterized by a free expansion with a linear behaviour ($R \approx t$); an intermediate stage where there is the shock wave formation and the plasma dynamics behaves as $R \approx t^{2\backslash5}$; and a final stage where the plasma expansion stops. These regimes that depend on the different process conditions are also temporally unified so that a single analytical curve gives a complete description of the phenomenon.

Experimentally, the chemical nature of the background gas, its pressure and the plasma energy can determine the occurrence of one or more of these regimes and a family of R-

t curves can be obtained. If these *R-t* experimental data are expressed in terms of the following dimensionless variables:

$$\widetilde{R} = R\left(\frac{2E}{P_o}\right)^{-1/3}; \widetilde{t} = t\upsilon_s\left(\frac{2E}{P_o}\right)^{-1/3} \tag{5}$$

where υ_s is the sound velocity in the ambient gas, P_0 is the known pressure of the gas and E is the total energy of the plasma, then all of points will fall into a single curve. The energy of the plasma E depends on the coupling between the laser pulse and the target material and it is just a fraction of the laser energy.

In this work we adopt this latest approach to explain our results: we express all experimental data in dimensionless variables according to Arnold et al. [16] model.

Depending on the adopted experimental conditions all of the three stages, free expansion ($R \approx t$), shock can be formation ($R \approx t^{2\backslash5}$) and the onset of the plume stopping were observed. Estimates of the plasma energy values can be also obtained from Eq. (5) applied to the R-t data in a limited range, i.e. where the ideal shock wave behaviour can be observed.

Among the wide class of complex rare earth nickel oxides, the present work focused on $Sm_{0.55}Nd_{0.45}NiO_3$ solid solution compound, corresponding to a T_{MIT} of about 37ºC [4], which allow room temperature applications. We report on its pulsed laser deposition and fast imaging. The approach presented here, allows investigating two main distinct aspects of pulsed laser deposition process i.e. the plume expansion and the film growth, thus highlighting the direct correlations among them. Such correlated study provides the opportunity of gaining a deeper understanding of the effect of the various processing parameters on the final film quality, allowing a fine tailoring of the experimental conditions in view of the desired film properties. Such quantitative approach to pulsed laser deposition is particularly relevant in the case of complex rare earth nickel oxides, since it is known that their properties can be modified in a dramatic way by minor structural tuning.

Experimental details

The experimental details for the target preparation and films deposition are reported in our previous work [26]. However, the targets were mounted in the vacuum system with a base pressure of 2.0 x 10^{-6} mbar, and ablated with KrF excimer laser at 45 degree incidence "Lambda Physik LPX-305icc having a wavelength $\lambda= 248$ nm" at a repetition rate of 3 Hz with an energy of 270 mJ on a spot size of 0.135 cm^2 that give a laser

fluence of 2 J/Cm2. Prior to the deposition, the substrates of size of 10x10x0.5 mm, were cleaned ultrasonically and then degreased in acetone. The substrates were mounted on a heated stage kept at 675 °C for the whole duration of the deposition process. This heating temperature was measured by a thermocouple located onto the substrate surface. The substrates - target distance was kept at 30 mm and the laser was focused to ablate the off-centre of the rotating target. Deposition was carried out onto different substrates: pure Si (100) and $NdGaO_3$. For the study of the plasma dynamics a set of spherical and plane mirrors and a Zeiss lens (76-mm focal length, spectral response: 350-800 nm) are used to form a two dimensional image of the luminous plasma on the intensified-charge-coupled-device (ICCD) camera (Princeton Instruments PI-MAX, 1024 × 256 pixels, pixel size = 26 × 26 µm). The temporal resolution of the ICCD camera is 5 ns and its spectral response is within the range of 190-850 nm. The observation was made along the normal to the ejected material direction of propagation. The number of accumulation, ICCD gain and gate are adjusted for each image to compensate the reduction of the plume intensity during the expansion. The target surface and the end of the laser pulse were tacked as the origin of distances and time delays.

Results and Discussions

We presented in our previous work a complete study of the evolution of the crystalline state and surface morphology of PLD grown of $Sm_{0.55}Nd_{0.45}NiO_3$ films as a function of O_2 pressure and also deposition time [26]. This study led to the determination of conditions that produce the growth of dense, uniform, and relatively smooth of $Sm_{0.55}Nd_{0.45}NiO_3$ films. The direct dependence of O_2 pressure on the evolution of the crystalline state and surface morphology of PLD grown $Sm_{0.55}Nd_{0.45}NiO_3$ films respectively on Si (100) and $NdGaO_3$ was demonstrated.

On Si (100), $Sm_{0.55}Nd_{0.45}NiO_3$ films of single phase are stabilized at an O_2 pressure of 0.4 mbar and present a very smooth surface characteristic; additional phase starts to appear when the O_2 pressure decreased from 0.4 to 0.1 mbar. While in the case of $NdGaO_3$, the $Sm_{0.55}Nd_{0.45}NiO_3$ is directly obtained. Films on $NdGaO_3$ systematically present only one phase corresponding to the stabilisation of the $Sm_{0.55}Nd_{0.45}NiO_3$ solid solution, with a net preferential crystal planes growth and the corresponding surface presents a roughness which is increasing with the deposition time. The direct stabilisation of the $Sm_{0.55}Nd_{0.45}NiO_3$ phase on $NdGaO_3$ without any additional phase at lower oxygen pressure of 0.2 mbar may be due to the effect of chemical pressure induced by the substrate.

The surface morphology of the different samples shows a net dense film structure with several droplets population. The nano-scaled droplets are in general spherical in shape which indicates that the laser ablation of this nickelate family may be governed to a certain extent by a heat transfer phenomenon.

In order to better understand the effect of oxygen pressure on the structural and morphological properties of the deposited $Sm_{0.55}Nd_{0.45}NiO_3$ thin films, we have studied the plasma plume dynamic of $Sm_{0.55}Nd_{0.45}NiO_3$ generated by laser ablation. The temporal evolution of the expanding plasma plume of $Sm_{0.55}Nd_{0.45}NiO_3$ into vacuum and some representative oxygen pressures is shown in Fig.1. Each image represents the spectrally integrated emission in the range of 400-800 nm of the plasma plume excited species. First, the images show that in the earlier time the expansion is mono-dimensional in the normal direction to the target. After a few hundred of nanoseconds the pressure gradients equilibrate and the plume extends in the three directions. This effect is more apparent in vacuum and lower oxygen pressure. Another feature to notice is the splitting of the plasma plume into two components at time delays and distances depending on the gas pressure. This marks the beginning of the interaction between the ejected species and the background gas molecules and the formation of a shock front. For 0.1 and 0.4 mbar the second component appears around 500 and 450 ns, respectively. For less than 0.1 mbar and more than 0.4 mbar, it is difficult to distinguish these two components.

The plume splitting appears only above a certain threshold pressure, this occurs at around 2×10^{-2} mbar. For more than 0.8 mbar it is very difficult to distinguish the two components this may be due to the confinement of the plasma by the gas. As the time evolves, the second component (the slower one) joins the first component because of the background gas braking of the latter, and the plume splitting disappears. The plume splitting has also been reported by several authors [27-31]. S Lafane et al. observed by fast imaging during the laser ablation of $Sm_{1-x}Nd_xNiO_3$ target in background oxygen pressure, the plume splitting at time delays for which the plume front still follows an almost free-plume expansion. This splitting is explained as a result of the interaction between the plume species which are scattered in backward direction after collisions with background gas molecules and the incoming particles. As time evolves and for some range of pressures, at around 0.4 mbar, a sharpening of the plume appears. This plasma sharpening was reported in [27] by S. Lafane et al. around 0.5 mbar and along with the sharpening, they observe a second splitting of the plasma into two components. This second splitting was clearly observed at 0.5-5 mbar pressure range in their data, however we were not able to see it clearly in our experimental data.

Plume sharpening behaviour suggests that high kinetic energy particles are emitted closer to the target surface normal [31]. It was attributed to the deceleration of a part of the plasma plume due to the interaction with background gas [28] or due to the formation of molecular species as reported by Kushwaha et al. [32]. Later on, a luminous point appears on the target surface. This emission comes from hot particles emitted by the target surface [33] and it's time of occurrence depends on the pressure.

In order to study the plasma plume expansion dynamics, we have plotted the plume luminous front position versus time delay at different pressures and under vacuum (see Fig. 2A and B). By increasing the oxygen pressure, the expansion remains linear in the early time.

From vacuum to 0.2 mbar no significant change in the initial velocity was observed. We estimated this velocity to be around 1.79×10^4 m/s. From 0.3 to 0.8 mbar the initial velocity decreased from 1.65×10^4 to 1.39×10^4 m/s. The deviation evolves with increasing time, from free-plume expansion to plume slowing down. In this regime of propagation, the ejected species collide with gas molecules and lose their kinetic energy. Later, the plume front stops completely (Fig. 2). At this stage, the ejected species diffuse into the ambient gas until they reach a distance where they lose their kinetic energy. The transition from one expansion regime to the next occurs at different time delays and distances depending on the gas pressure. As discussed above several models have been proposed to describe the ablation plume expansion in a background gas. The deviation from the free-plume expansion and the appearance of luminous layer in the plasma-gas interface marks the presence of a shock wave front. We used different model to fit our experimental data in order to verify their validity. The results are shown in Figure 3 and the fitting parameters are reported in Table 1.

It was found that for all used pressures the shock wave model fit agree well only with some of our experimental data and in a range of pressures. At 0.2, 0.3, 0.4 and 0.8 mbar the lower limit of the deviation from the free-plume expansion to the shock-wavelike expansion, is 9, 8.15, 8.06 and 9.5 mm (see fig. 3 C, D, E and F), respectively. At lower pressures, the shock wave model does not fit well with our experimental data but the drag model agreed well from the deviation of a free-plume expansion (see Fig. 3 A and B).

Thus, the deviation from the free-plume expansion to the shock-wave-like expansion becomes abrupt as we increase the oxygen pressure. It is to be noticed that as the distances, the lower and the higher limit of time delays where the shock-wave model is

8

valid, decrease by increasing the gas pressure from 0.2 to 0.4 mbar. Above 0.4 mbar the distances of the lower and the higher limit of the time delays where the shock wave model is valid increase again. As function of time, there is an anomaly on the lower and higher time delay limit of the shock-wave model validity. At 0.2, 0.3, 0.4 and 0.8 mbar the lower time delay limit are 522, 452, 537 and 723 ns while the higher time delays limit are 2087, 2500, 2300 and 2900 ns respectively.

According to Zel'dovich and Raiser [25], shock-wave formation becomes important when the mass of the displaced gas is comparable to the masse of the plasma (Mp). Assuming a hemispherical expansion of the plume, using the drag model and taking R_{sw} as the front position at which the beginning of the shock-wave formation was observed, Mp was calculated in [27] by S. Lafane et al. for all the used pressures and compared to the measured ablated. Thier Mp calculated values are closed to thier measured value particularly at pressures between 0.3 and 1 mbar and this agreed well with our experimental data as in this range of oxygen pressure the expansion become more hemispherical and closer to the ideal shock wave model as demonstrated in the fitting parameters reported in Table 1.

As mentioned above using a shock-wave model, only a limited oxygen pressure and region of the experimental data are well fitted. At longer time delays the measured distances value are smaller than those predicted by shock-wave model. In this stage, the drag model can be used to describe the behaviour of the plume expansion [28, 29].

This model predicts that the plume will come to rest due to resistance from collisions with the background gas. The drag model fits very well our experimental data at later time delays for all the used oxygen pressure. According to Amoruso et al. [30, 34, 35] and J. Schou [36] the plume stops when the shockwave gradually degenerates into a sound wave in the undisturbed gas, and almost all the energy initially stored in the plume is converted into a sound wave propagating in the ambient gas. In Table 1, the observed plume stopping distance versus oxygen gas pressure can be evaluated from the equation of the drag model. The stopping distance decreases from 35 mm to about 20.6 mm for 0.02 and 0.8 mbar respectively.

Arnolds et al. [16] gave a more general description to the plume dynamics into background gas pressure using dimensionless distance-time variables. The model proposed describes the different stages of the plume expansion: the free expansion; the shock-wave-like expansion and finally the plume stopping. As it is illustrated in Fig. 2B where the data reported in Fig. 2A are plotted in terms of the dimensionless variables, all the curves for different pressures collapse onto almost single curve at the earlier time

of propagation and where the shock wave model was valid. As the times involves we can notice the deviation from the ideal shock wave expansion model when decreasing the pressure and this mark the interactions between the gas and the plasma plume and the formation of the shock wave along with the increase of the oxygen pressure.

The study on plume dynamic shows that the plasma plume expansion dynamic passes from free-like to shock-like and finally reaches a complete stopping at times and distances depending on the gas pressure. It was found that the validity of the shockwave model is restricted to a distance region which depends on the gas pressure. A drag model is a good approximation for the later plume expansion regime. An optimal target substrate distance was predicted for each gas pressure based on the plasma plume stopping distance. This study on plasma expansion demonstrates in direct dependence on O_2 pressure of the evolution of the crystalline state and surface morphology of PLD grown $Sm_{0.55}Nd_{0.45}NiO_3$ films through the formation of the shock wave. On the basis of these data and in correlation with our previous work [26], it has to be noticed that the morphology feature where all films show a similar behaviour as a function of pressure [26], can be related to the diffusion of the plasma species as the films were deposited at distance above the estimated stopping distance of the plasma. On Si (100) substrate, Sm0.55Nd0.45NiO3 films single phase are stabilized at an O_2 pressure of 0.4 mbar and present a very smooth surface characteristic, while an additional phase starts to appear when the O_2 pressure decreased from 0.4 to 0.1 mbar [26]. In the case of $NdGaO_3$ substrate, the $Sm_{0.55}Nd_{0.45}NiO_3$ thin films are directly obtained and films systematically present only one phase corresponding to the stabilization of the $Sm_{0.55}Nd_{0.45}NiO_3$ solid solution, with a net preferential crystal planes growth and the corresponding surface shows a roughness which increases with the deposition time. The direct stabilization of the $Sm_{0.55}Nd_{0.45}NiO_3$ phase without any additional phase may be due to the effect of chemical pressure induced by the substrate [26].

Conclusion

The results are reported and discussed in the framework of a specific aspect focusing at the best conditions which can be used to optimize the synthesis of $Sm_{1-x}Nd_xNiO_3$ at x= 0.45 solid solution . In particular we report on some fast photography imaging studies of the plasma generated by the KrF excimer laser ablation of $Sm_{1-x}Nd_xNiO_3$ at x= 0.45 in the presence of oxygen background gases at different pressures. The experimentally determined behavior is compared with the predictions of an analytical model which gives a complete description of the expansion of the plume and with some recent results reported in the literature. Evidence of the strong influence of the expansion plasma

regime is found which showed that it is not simply related to the overall reactive gas content.

Acknowledgment.

References

[1]   M. L. Medarde; J. Phys.: Condens. Matter; 9, 1679 (1997)

[2]   P. Lacorre, J. B. Torrance, J. Pannetier, A. J. Nazzal, P. W. Wang and T. C. Huang; J. Solid State Chem.; 91, 225, (1991)

[3]   F. Capon, P. Laffez, J. F. Bardeau, P. Simon, P. Lacorre and M. Zaghrioui; Appl. Phys. Lett.; 81, 619 (2002)

[4]   A. Ambrosini and J. F. Hamet; Appl. Phys. Lett.; 82, 727 (2003)

[5]   F. Capon; PhD Thesis University of Maine; France (2003)

[6]   J. B. Torrance, P. Lacorre, A. I. Nazzal, E. J. Ansaldo and Ch. Niedermayer; Phys. Rev. B; 45, 8209 (1992)

[7]   R. D. Sanchez, M. T. Causa, A. Seoane, J. Rivas, F. Rivadulla, M. A. Lopez-Quintela, J. J. Perez Cacho, J. Blasco and J. Garcia; J. Solid State Chem.; 151, 1, (2000)

[8]   D.B. Geohegan, Appl. Phys. Lett. 60, 2732 (1992)

[9]   D.B. Geohegan, Appl. Phys. Lett. 67, 197 (1995)

[10]   H.-j. Dang, Q.-z. Qin, Appl. Surf. Sci. 151, 180 (1999)

[11]   S.S. Harilal, C.V. Bindhu, M.S. Tillak, F. Najmabadi, A.C. Gaeris, J. Appl. Phys. 93, 2380 (2003)

[12]   S. Amoruso, A. Sambri, X. Wang, J. Appl. Phys. 100, 013302 (2006)

[13]   S. Amoruso, J.Schou, J. G. Lunney, Appl. Phys. A 92, 907 (2008)

[14]   S. I. Anisimov, B.S. Luk'yanchuk, A. Luches; Appl. Surf. Sci., 96-98 (1996)

[15]   R. K. Singh, J. Narayan, Phys. Rev. B, 41, 8843 (1990)

[16]   N. Arnold, J. Gruber, J. Heitz Appl. Phys.A 69 S 87-93 (1999)

[17]   M. R. Predtechensky and A. P. Mayorov, Appl. Supercond. 1, 10, 2011 (1993)

[18]   T.E.Itina, A. A. Katassonov, W. Marine M. Autric J.Appl.Phys. 83, 11 6050 (1998)

[19]   H.J. Dang, M.F. Zhou, Q.Z. Qin, Appl. Surf. Sci. 140, 118 (1999).

[20]   M. Okhoshi, T. Yoshitake, K. Tsushima, Appl. Phys. Lett. 64, 3340 (1994).

[21] W.K.A. Kumuduni, Y. Nakayama, Y. Nakata, T. Okada, M. Maeda, J. Appl. Phys. 74, 3340 (1993).

[22] D.B. Chrisey, G.K. Hubler, D. Geoheagan, Pulsed Laser Deposition of Thin Films (Wiley, New York 1994) Chap.5.

[23] J. Gonzalo, C.N. Afonso, I. Madariaga, J. Appl. Phys. 81 951 (1997).

[24] P.E. Dyer, A. Issa, P.H. Key, Appl. Phys. Lett. 57, 186 (1990).

[25] Y. B. Zel'dowich, Y. P. Raizer,Physics of Shock Waves and High Temperature Hydrodynamic Phenomena(Academic Press, New York 1966).

[26] B. D. Ngom, R. Madjoe, S. Fall, J. B. Kana kana, N. Manyala, A. Forbes, R. Nemetudi, A. Y. Fasasi, M. Maaza, and A. C. Beye, J. Phys. Chem. Solids, 71, 722-729 (2010)

[27] S. Lafane, T. Kerdja, S. Abdelli-Messaci, S. Malek, M. Maaza, Appl Phys A DOI 10.1007/s00339-009-5392-y

[28] S. S. Harilal, C.V. Bindhu, M.S. Tillak, F. Najmabadi, A.C. Gaeris, J. Appl. Phys. 93, 2380 (2003)

[29] D. B. Geohagan, Thin Solid Film 220, 138 (1992)

[30] S. Amoruso, A. Sambri, M. Vitiello, X. Wang, Appl. Surf. Sci. 252, 4712 (2006)

[31] S.S. Harilal, C.V. Bindhu, M.S. Tillack, F. Nadjmabadi, A.C. Gaeris, J. Appl. Phys. 93, 2380 (2002)

[32] A. Kushwaha, R.K. Thareja, Appl. Opt. 47, G65 (2008)

[33] P. Serra, L. Cléries, J.L. Morenza, Appl. Surf. Sci. 96–98, 216 (1996)

[34] S. Amoruso, R. Bruzzesi, N. Spinelli, R. Velotta, M. Vitiello, X. Wang, Phys. Rev. B 67, 224503 (2003)

[35] S. Amoruso, B.Toffman, J.Schou, Phys. Rev. E 69, 05643 (2004)

[36] J. Schou, Appl. Surf. Sci. 255, 5191 (2009)

Figures Captions

Figure 1

The temporal evolution of the visible plume of pulsed laser ablated $Sm_{0.55}Nd_{0.45}NiO_3$ target with 2 J/cm^2. The position of the ablating surface is at the limit of the top side of the images

Figure 2

Plume of pulsed laser ablated $Sm_{0.55}Nd_{0.45}NiO_3$ target with 2 J/cm^2 front position as a function of the time delay at different background oxygen pressure and in vacuum. The *solid lines* represent the free expansion fit.

Figure 3

Fits of the different models used to describe the plume expansion of pulsed laser ablated $Sm_{0.55}Nd_{0.45}NiO_3$ target with 2 J/cm^2 for different pressures. The *red line* represents the free expansion fit. The *green line* shows the shock-wave model fit. The *blue line* shows the drag model fit.

Figure 4

Plume of pulsed laser ablated $Sm_{0.55}Nd_{0.45}NiO_3$ target with 2 J/cm^2 front position versus time delay at different background oxygen pressures in the dimensionless variables

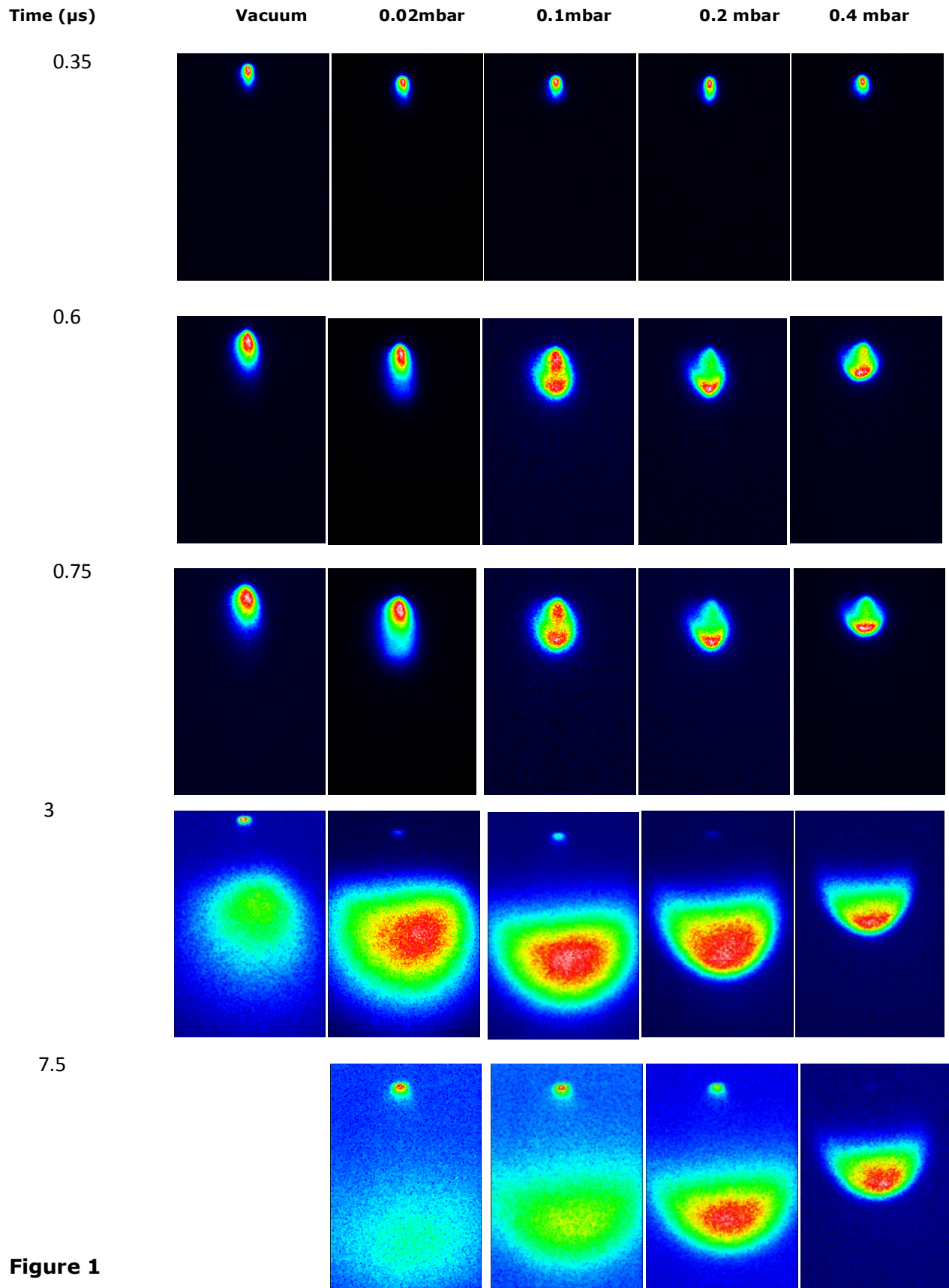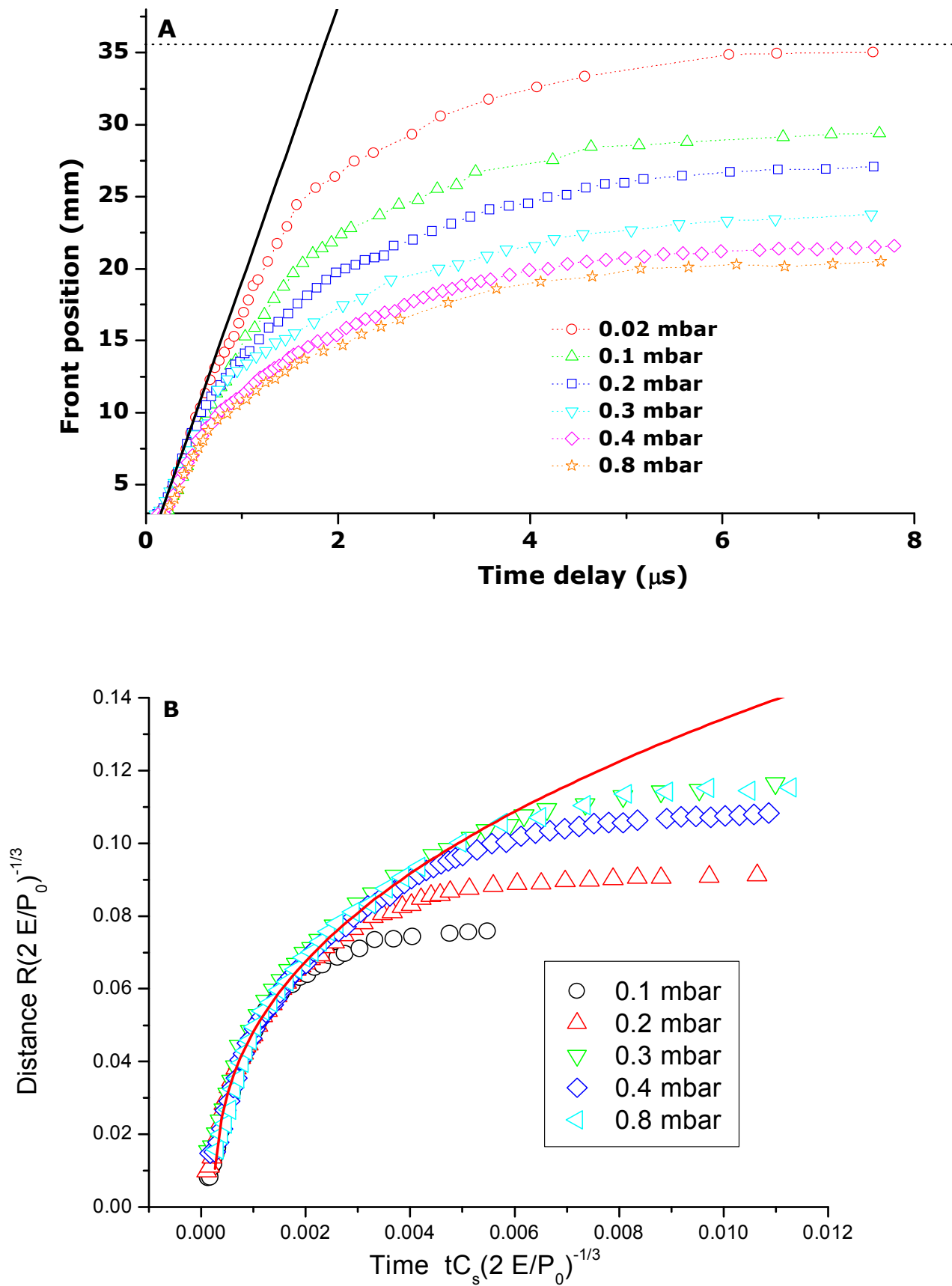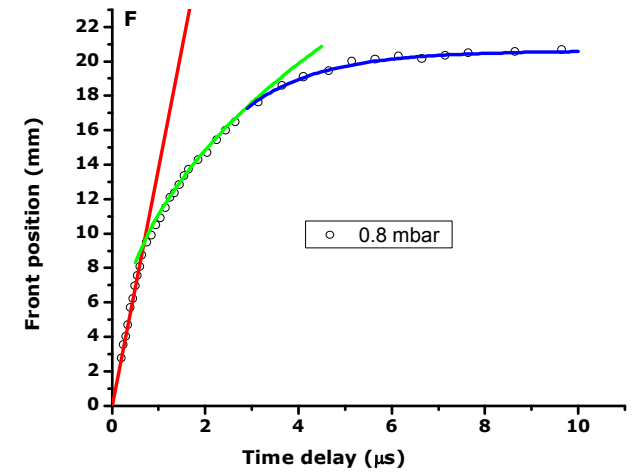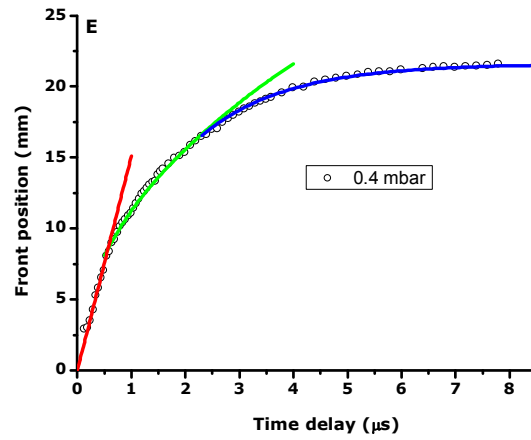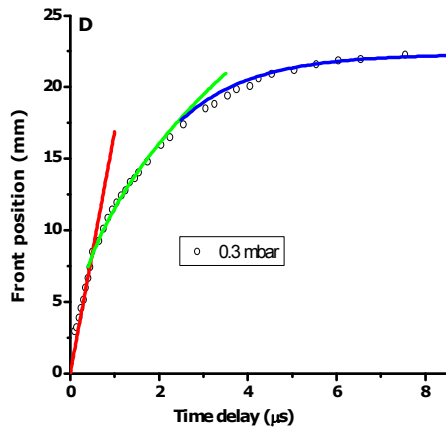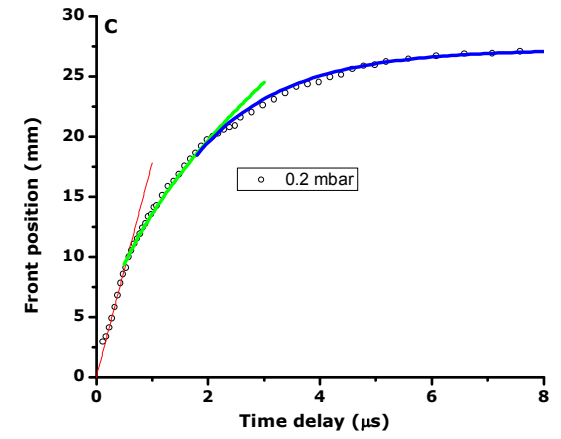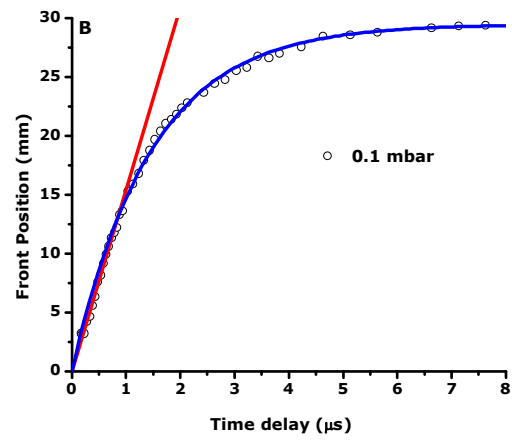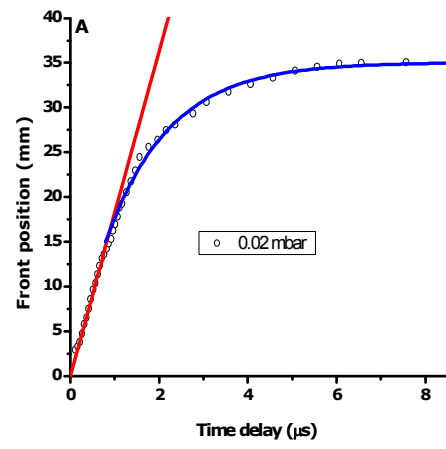| Time (μs)	Vacuum	0.02mbar	0.1mbar	0.2 mbar	0.4 mbar
0.35					
0.6					
0.75					
3					
7.5					

Figure 1

Figure 2

Figure 3

Table 1 The fitting parameters of the different model used to fit our experimental data

Pression (mbar)	Linear V_0 (X10^4 m/s)	Shock Wave Model: $p2$	$p1$	Drag Wave Model: R_o (cm)	β(x10^{11}m/s^2)
Vacuum	1.820	-	-	-	-
0.02	1.814	-	-	3.5	7
0.1	1.798	-	-	2.76	6.4
0.2	1.783	0.330	0.538	2.72	6.3
0.3	1.65	0.424	0.478	2.2	6.3
0.4	1.512	0.431	0.472	2.16	6.3
0.8	1.39	0.610	0.420	2.1	6.3